Editors' Suggestion   Featured in Physics

Guiding Dirac Fermions in Graphene with a Carbon Nanotube

Austin Cheng,[1] Takashi Taniguchi,[2] Kenji Watanabe,[2] Philip Kim,[1] and Jean-Damien Pillet[3,*]

[1]*Department of Applied Physics, Harvard University, Cambridge, Massachusetts 02138, USA*
[2]*National Institute for Material Science, Tsukuba 305-0044, Japan*
[3]*LSI, CEA/DRF/IRAMIS, Ecole Polytechnique, CNRS, Institut Polytechnique de Paris, F-91128 Palaiseau, France*

Relativistic massless charged particles in a two-dimensional conductor can be guided by a one-dimensional electrostatic potential, in an analogous manner to light guided by an optical fiber. We use a carbon nanotube to generate such a guiding potential in graphene and create a single mode electronic waveguide. The nanotube and graphene are separated by a few nanometers and can be controlled and measured independently. As we charge the nanotube, we observe the formation of a single guided mode in graphene that we detect using the same nanotube as a probe. This single electronic guided mode in graphene is sufficiently isolated from other electronic states of linear Dirac spectrum continuum, allowing the transmission of information with minimal distortion.

Like a photon, an electron can be used as a carrier of information [1]. However, there is a limited number of tools to control a single electron [2] and the simple fact of guiding it coherently in a solid, like an optical fiber for light, is a technological feat [3,4]. One-dimensional materials such as semiconducting nanowires naturally provide guidance for electrons, but in these materials, electrons can only be transmitted over short distances before losing its information [5]. Another possibility is through the edge channel of a two-dimensional electron gas in the quantum Hall regime, but a large magnetic field is required for the channel to be a single mode [6], which is crucial for the carried information not to be distorted during propagation.

An alternative approach, conceptually similar to an optical fiber [7], is to use an electrostatic potential well on a two-dimensional electron gas to confine the movement of electrons along one direction [Fig. 1(a)] [8–11]. Particularly, massless quasiparticles in graphene are an ideal platform for the realization of such electron guide. The quasirelativistic linear energy dispersion in graphene allows the wave function of the Dirac fermions travel with minimal distortion. Furthermore, it has been demonstrated that high mobility [12] allows electrons to be transmitted ballistically over several microns even at room temperature [13]. In addition, graphene can be encapsulated between thin dielectric layers of hexagonal-boron nitride (h-BN) [14], providing tunable electrostatic potential on the scale of a few nanometers, without degradation of the mobility. Electrostatic gating has produced various electron-optical elements, including lenses with negative refractive index [15] and filter-collimator switches [16].

An ideal single mode electronic guide requires a deep potential well with a width much smaller than the
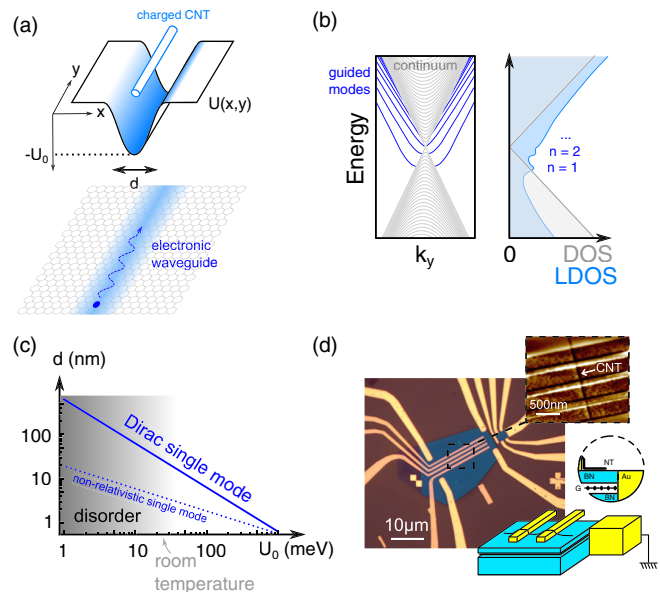

FIG. 1. Electron waveguide in graphene. (a) Schematic of graphene with a potential well represented by the blue region which confines electrons along the y direction. Below, electrostatic potential along the x direction generated by a charged carbon nanotube (CNT). (b) Schematic of the band structure as a function of momentum k_y. The gray lines correspond to the bulk states, and the blue lines correspond to the guided modes. On the right: global density of states (DOS) and local density of states (LDOS) as a function of energy. (c) Diagram showing the condition (blue line) for a waveguide to host a Dirac single mode and nonrelativistic single mode. (d) Optical image of one of the devices. EFM picture of a CNT on top of a h-BN encapsulated graphene device with metallic electrodes and a schematic of the device structure.

wavelength of electrons in order to suppress scattering in the core of the waveguide [17]. The wavelength can reach around 100 nm with experimentally accessible densities, and it is therefore crucial to be able to place extremely narrow gates close to the electron gas. The electronic modes generated by such a one-dimensional (1D) potential well are manifested in the band structure of the graphene as branches similar to optical modes, which are separated from the continuum up to the energy that roughly corresponds to the depth of the potential well U_0 [Fig. 1(b)]. Being isolated energetically, the guided modes are unlikely to mix with one another. Moreover, they are predicted to propagate ballistically over exceptional distance [18]. These modes form locally, at the center of the potential well, such that they do not affect the overall graphene density of states (DOS) but appear as resonances in the local density of states (LDOS) close to the LDOS minimum which indicates the position of the local Dirac point.

In this experiment, we use carbon nanotube (CNT) for creating 1D local gate to create a guiding mode in graphene by generating a potential well [Fig. 1(a)]. The depth of the potential well can be continuously adjusted by a voltage difference applied between the CNT and the graphene. The width d of the guided channel is roughly equal to the radius of the CNT, around 1 nm, plus the thickness of h-BN separating the CNT and graphene. The number of modes is then approximately given by the ratio $U_0 d / \hbar v_F$, where v_F is the Fermi velocity, and must, therefore, be of the order unity for a single mode waveguide [19,20]. In principle, this condition can be fulfilled for very wide and shallow potentials, but for the mode to be well defined it is necessary that the potential depth is much greater than the fluctuations of chemical potential caused by the disorder. This limitation explains in particular why it is difficult to guide electrons in disordered graphene. For graphene encapsulated in h-BN, these fluctuations are on the order of a few meV [21,22]. In order to obtain a single mode waveguide that is immune to disorder, the depth of the potential well, therefore, needs to be around a few tens of meV, which requires a width on the order of 10 nm [Fig. 1(c)]. Such conditions are very hard to fulfill with standard techniques of nanofabrication but are conceivable using a gate made with a single-walled CNT in close proximity to graphene. We also note that the linear dispersion of Dirac fermion graphene is essential for our experiment. For nonrelativistic electrons in semiconductors, the criterion to have a single mode is $U_0 d^2 \ll h^2/m$, where m is the effective mass, leading to a much shallower potential well ($\sim$meV) even for smaller width $d < 10$ nm [Fig. 1(c)].

An optical image of one of our devices is shown in Fig. 1(d). Graphene is encapsulated between two layers of h-BN where the upper one is only a few nm thick and on which a CNT is deposited. Since the CNT diameter lies between 1 and 3 nm, and the thickness of our top h-BN layer is only a few nanometers, the characteristic width of the well is around 10 nm or less. We are thus able to drive the device into a single guided mode formed in graphene beneath the CNT. The graphene and CNT are both connected to their own electrodes which allows them to be independently controlled and measured. The length of the waveguide here is defined by the distance between electrodes connecting the CNT, i.e., 500 nm. The details of fabrication are given in the Supplemental Material [23].

In addition to generating a potential well, the same CNT can also be used as a local probe to measure the graphene LDOS utilizing the capacitive coupling between CNT and the guided modes in the graphene. Here we operate the CNT as a single electron transistor (SET), i.e., a charge sensor [27]. Figure 2(a) shows a schematic of the measurement scheme where the electrostatic potential of CNT SET can be controlled by both graphene gate voltage (V_G) and the global back gate voltage (V_{bg}). When connected to metallic electrodes and at sufficiently low temperature, a CNT generally enters the Coulomb blockade regime and becomes sensitive to external charges [28]. By measuring the conductance G_{NT} of the CNT as a function of the gate voltage V_{bg} or the potential applied to the graphene sheet V_G, we observe a series of peaks corresponding to the different electronic energy levels of the CNT [Fig. 2(a), bottom panel], each of which can contain one electron. These energy levels can individually be used as local probes sensitive to the electrostatic environment and therefore to the local charge density of graphene located below the CNT. The operational principle of these probes, inspired by direct measurements of Fermi energy performed in graphene and bilayer graphene [29,30], is illustrated in Fig. 2(b). When increasing the back gate potential V_{bg}, we fill the graphene band structure by increasing the number of carrier by δn_G with the corresponding change of Fermi energy δE_F. If the total electrochemical potential of graphene (electrostatic potential added to the Fermi energy E_F) exceeds the energy of one of the electronic states of the CNT, then the latter is also filled. Subsequently, we lower the graphene electrostatic potential with V_G and therefore reduce the energy of all the electrons in graphene by an amount δE_F. If μ, adjusted by a change of the graphene bias δV_G, becomes lower than the energy of the same CNT electronic level, it consequently empties and goes back to its original state. By measuring the charge state of the CNT between each step, it is then possible to deduce the energy change $\delta E_F = e \delta V_G$ corresponding a charge variation δn_G, where e is the charge of an electron. This procedure yields the local quantum capacitance of graphene

$$C_q = e^2 \frac{\delta n_G}{\delta E_F}.$$

Note that the quantum capacitance at finite temperature is related to the compressibility of a mesoscopic system $C_q = e^2 \partial n_G / \partial \mu$, which can be associated with the many
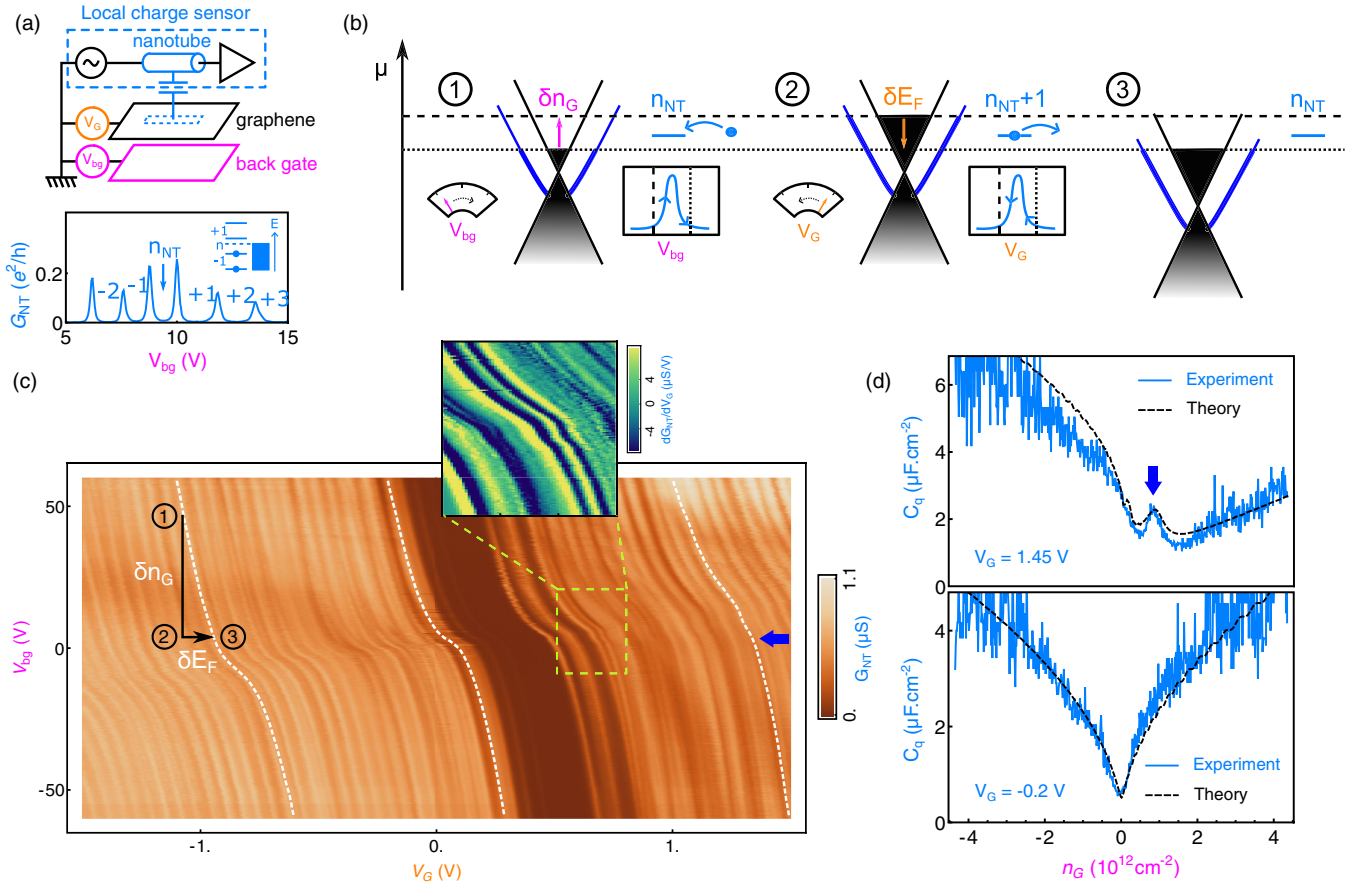
FIG. 2. Graphene density of states measured with the carbon nanotube (CNT). (a) Schematic of the measurement setup (top) and CNT conductance measured as a function of the backgate showing the Coulomb blockade behavior. All measurements presented in this Letter are performed at 1.6 K. (b) Operational principle of the CNT sensor. (c) CNT conductance G_{NT} vs V_G and V_{bg}. The wide dark brown area around $V_G = 0$ corresponds to the semiconducting gap of the CNT, in which the latter is not charged. Inset shows dG_{NT}/dV_G over a small region in order to highlight a double kink corresponding to the Dirac point followed by a guided mode resonance (blue arrow). (d) Local quantum capacitance measured as a function of global charge carrier density n_G for two different voltage differences V_G between the CNT and graphene.

body DOS [31]. Since capacitive coupling between graphene and CNT is strongly localized vicinity of the CNT, the measured C_q is proportional to the LDOS of graphene underneath the CNT. This quantity cannot be obtained with a global transport measurement. A remarkable aspect of this technique is that it provides an absolute measurement of quantum capacitance without any scaling parameters or adjustment of the origin of energies.

Figure 2(c) shows the conductance of the CNT G_{NT} as a function of V_{bg} and V_G. For this particular device, the h-BN spacer between CNT and graphene is only 4 nm thick, the measured peaks in the G_{NT} exhibit trajectories in the V_{bg}-V_G plane that yields the evolution of the Fermi energy as we described above. The slope of these trajectories gives us directly the local quantum capacitance C_q. When $V_G \approx 0$, the potential difference between the CNT and the graphene is small and, consequently, the potential well generated by the presence of the CNT is shallow. The LDOS measured [Fig. 2(d)] is then the one of bare

graphene with a minimum at zero energy, following $|n_G|^{1/2}$ on the hole and electron sides. Note that n_G denotes the global charge density of graphene since V_{bg} controls the charge density over the entire graphene sheet. With the minimum of LDOS being very close to $n_G = 0$, we deduce that the doping underneath the CNT is low, suggesting a locally low impurity levels. The minimum value of $C_q \sim 0.5\ \mu\mathrm{F\,cm^{-2}}$ also gives an estimation of the attainable minimal charge carrier concentration due to the charge puddle disorders $\sim 10^{10}\ \mathrm{cm^{-2}}$.

As we generate a deeper potential well by increasing V_G, the LDOS develops a more pronounced characteristic resonance, corresponding to a single guided mode. Compared to the measurement performed at $V_G = 0$, the minimum of quantum capacitance has shifted from the global charge neutrality point and toward the electron side ($n_G > 0$), as expected for a positive voltage applied on graphene while the CNT is maintained at ground potential. The resonance lies between this minimum and the global
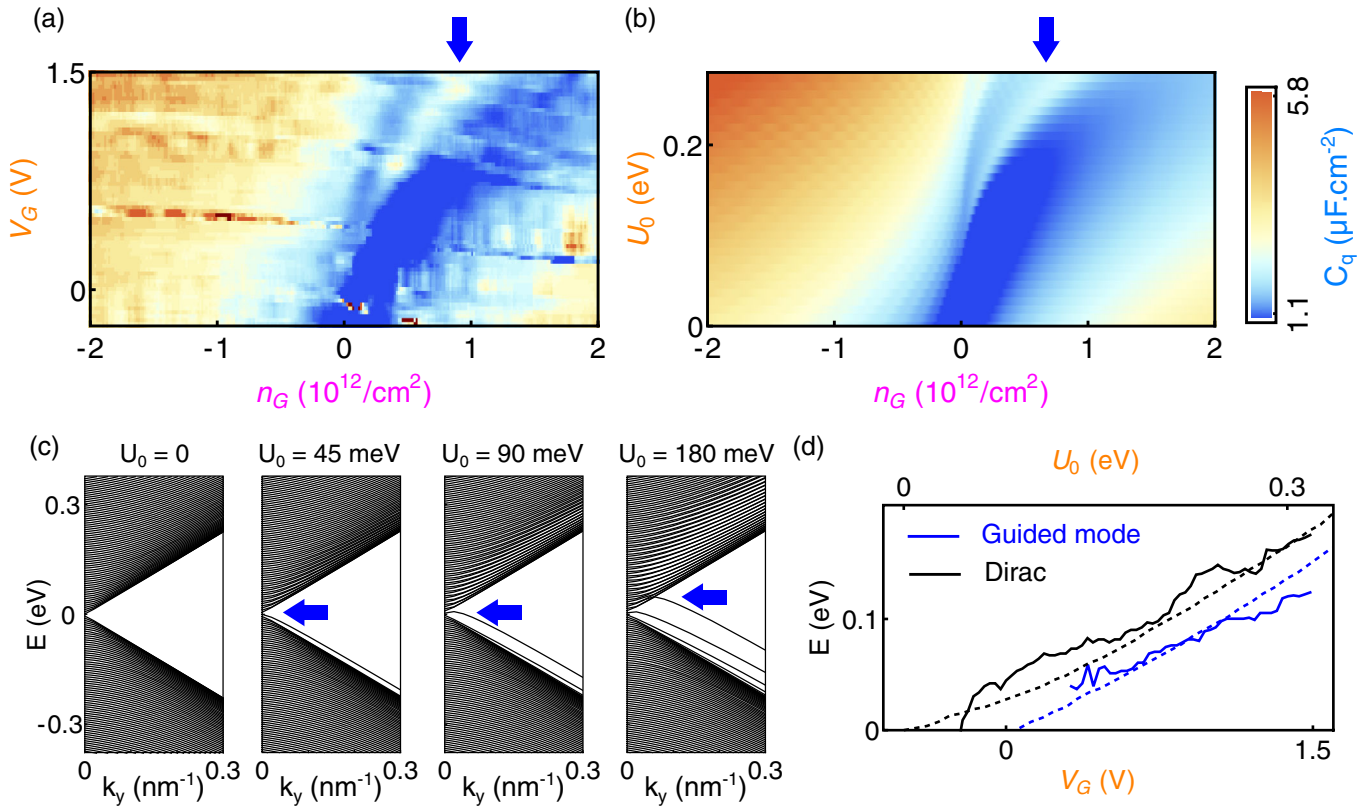
FIG. 3.   Potential depth dependence. (a) Evolution of the graphene local density of states with the potential well depth U_0 controlled by V_G. (b) Comparison with theoretical calculations obtained from a tight-binding modeling. (c) Theoretical evolution of the band structure for increasing U_0. (d) Positions of local Dirac point and first guided mode as a function of V_G (experiment: continuous lines) and U_0 (theory: dashed lines). Here, the scales of U_0 and V_G are adjusted to show the apparent linear relation between U_0 and V_G in the accessible gate voltage range where the guided mode forms.

charge neutrality point of graphene ($n_G = 0$), a region where the a region where the doping caused by the potential well actually leads to an n-p-n junction configuration, where n(p) refers to negative (positive) charge density. The appearance of this resonance can be understood in the following manner: as a guided mode detaches from the Dirac cone, it generates a peak in the LDOS due to the 1D van Hove singularity appearing at the extrema of the single mode energy dispersion $E(k_y)$ where k_y is the wave vector along the CNT [see Fig. 3(c)]. Our measurements are in excellent agreement with numerical tight-binding simulations [32,33] where the only fitting parameters are the depth and width of the potential well (see the Supplemental Material [23]). Theory predicts the appearance of multiple successive modes that could give rise to additional resonances [34]. However, due to presumably disorder induced broadening, unambiguously identifying multiple resonances is challenging within our experimental noise limit.

We observe a continuous evolution from bare graphene to a single mode waveguide as we tune the potential depth U_0. Measurements of Fig. 3(a) show that the graphene LDOS appears to be dramatically affected by tuning U_0, by changing the potential difference V_G between the CNT and graphene becomes nonzero. At low U_0, it is already

clear that the minimum corresponding to the Dirac point is less pronounced and that an asymmetry is formed between the electron and hole sides. This evolution, also predicted by numerical simulations [Fig. 3(b)], is due to the formation of closely packed guided modes whose branches are too close to the continuum, preventing the development of sharp resonances in the LDOS. Figure 3(c) shows computed dispersion relation as a function of k_y momentum along the CNT direction. A branch corresponding to the 1D guided mode gradually and continuously separates from the Dirac cone as U_0 increases [19]. For larger V_G, we start to observe a resonance gradually increasing in amplitude and shifting from the charge neutrality point. This reflects the formation of a branch in the dispersion relation of graphene, which becomes increasingly more detached from the continuum. The curvature of this branch at its beginning becomes flat [19] until it acquires a minimum located around $k_y \approx 1/d$, giving rise to a sharp resonance in LDOS. In the relativistic Dirac fermionic system, the 1D guide mode is expected to exhibit a potential strength threshold for the appearance of the first guided mode [20,35]. While Fig. 3(d) suggests that indeed the appearance of a guided mode starts at finite U_0, further experimental study with higher resolution requires to prove such threshold behavior

unambiguously. Among all our devices, we were able to observe a single guided mode in the ones with upper h-BN that are 6 nm or thinner. In devices made with a thicker upper h-BN layer, from 10 to 100 nm, we were only able to observe the asymmetry between electron and hole sides but no resonance in the LDOS (see the Supplemental Material [23]). This experimental observation confirms that we cannot create a robust single mode electronic waveguide if the well is too wide and underlines the importance of the CNT for the realization of the single guided mode.

Technological applications for guided modes are possible if the energy separations between their branches and the continuum are sufficiently large. Indeed, to make the information transmission robust along the guide, it is necessary to avoid processes that scatter electrons, leading to loss of information. For applications operating at room temperature, this energy must be well above thermal energy 25 meV. This separation is directly given by the energy position of the resonance with respect to the global Dirac point of graphene. Though our measurement technique does not work at room temperature since it relies on Coulomb blockade, we can see on the curve of Fig. 3(d) that we can control this energy continuously up to approximately 0.1 eV, well above thermal fluctuations at room temperature. This suggests that such guided modes could have great potentials to be used as novel electronic devices analogous to optical ones but where carriers of information are electrons rather than light. Additional measurements need to be performed at room temperature to confirm this hypothesis. Complementary measurements based on infrared nanoimaging [36], scanning tunneling spectrocopy [2,37,38], or planar tunneling spectroscopy [39] with a 1D local gate created by a nanotube underneath the junction could also bring precious insight on the coherence, robustness, and physical properties of these guided modes. More generally, guided modes in Dirac materials are also of interest for plasmonics applications [36,40,41], ultrafast electronic [42], spintronics [43], or to be used as test beds for relativistic simulation [44–46].

---

[*]jean-damien.pillet@polytechnique.edu

[1] C. Bäuerle, D. C. Glattli, T. Meunier, F. Portier, P. Roche, P. Roulleau, S. Takada, and X. Waintal, Rep. Prog. Phys. 81, 056503 (2018).

[2] Y. Zhao, J. Wyrick, F. D. Natterer, J. F. Rodriguez-Nieva, C. Lewandowski, K. Watanabe, T. Taniguchi, L. S. Levitov, N. B. Zhitenev, and J. A. Stroscio, Science 348, 672 (2015).

[3] J. R. Williams, T. Low, M. S. Lundstrom, and C. M. Marcus, Nat. Nanotechnol. 6, 222 (2011).

[4] P. Rickhaus, M.-H. Liu, P. Makk, R. Maurand, S. Hess, S. Zihlmann, M. Weiss, K. Richter, and C. Schönenberger, Nano Lett. 15, 5819 (2015).

[5] S. Chuang, Q. Gao, R. Kapadia, A. C. Ford, J. Guo, and A. Javey, Nano Lett. 13, 555 (2013).

[6] P. Rickhaus, P. Makk, M.-H. Liu, E. Tóvári, M. Weiss, R. Maurand, K. Richter, and C. Schönenberger, Nat. Commun. 6, 6470 (2015).

[7] D. Gloge, Appl. Opt. 10, 2252 (1971).

[8] F.-M. Zhang, Y. He, and X. Chen, Appl. Phys. Lett. 94, 212105 (2009).

[9] Y. Jompol, C. J. B. Ford, J. P. Griffiths, I. Farrer, G. a. C. Jones, D. Anderson, D. A. Ritchie, T. W. Silk, and A. J. Schofield, Science 325, 597 (2009).

[10] R. R. Hartmann, N. J. Robinson, and M. E. Portnoi, Phys. Rev. B 81, 245431 (2010).

[11] Z. Wu, Appl. Phys. Lett. 98, 082117 (2011).

[12] C. R. Dean, A. F. Young, I. Meric, C. Lee, L. Wang, S. Sorgenfrei, K. Watanabe, T. Taniguchi, P. Kim, K. L. Shepard, and J. Hone, Nat. Nanotechnol. 5, 722 (2010).

[13] A. S. Mayorov, R. V. Gorbachev, S. V. Morozov, L. Britnell, R. Jalil, L. A. Ponomarenko, P. Blake, K. S. Novoselov, K. Watanabe, T. Taniguchi, and A. K. Geim, Nano Lett. 11, 2396 (2011).

[14] L. Wang, I. Meric, P. Y. Huang, Q. Gao, Y. Gao, H. Tran, T. Taniguchi, K. Watanabe, L. M. Campos, D. A. Muller, J. Guo, P. Kim, J. Hone, K. L. Shepard, and C. R. Dean, Science 342, 614 (2013).

[15] S. Chen, Z. Han, M. M. Elahi, K. M. M. Habib, L. Wang, B. Wen, Y. Gao, T. Taniguchi, K. Watanabe, J. Hone, A. W. Ghosh, and C. R. Dean, Science 353, 1522 (2016).

[16] K. Wang, M. M. Elahi, L. Wang, K. M. M. Habib, T. Taniguchi, K. Watanabe, J. Hone, A. W. Ghosh, G.-H. Lee, and P. Kim, Proc. Natl. Acad. Sci. U.S.A. 116, 6575 (2019).

[17] M. T. Allen, O. Shtanko, I. C. Fulga, A. R. Akhmerov, K. Watanabe, T. Taniguchi, P. Jarillo-Herrero, L. S. Levitov, and A. Yacoby, Nat. Phys. 12, 128 (2016).

[18] O. Shtanko and L. Levitov, Proc. Natl. Acad. Sci. U.S.A. 115, 5908 (2018).

[19] C. W. J. Beenakker, R. A. Sepkhanov, A. R. Akhmerov, and J. Tworzydło, Phys. Rev. Lett. 102, 146804 (2009).

[20] H. C. Nguyen, M. T. Hoang, and V. L. Nguyen, Phys. Rev. B 79, 035411 (2009).

[21] J. Xue, J. Sanchez-Yamagishi, D. Bulmash, P. Jacquod, A. Deshpande, K. Watanabe, T. Taniguchi, P. Jarillo-Herrero, and B. J. LeRoy, Nat. Mater. 10, 282 (2011).

[22] M. Yankowitz, Q. Ma, P. Jarillo-Herrero, and B. J. LeRoy, Nat. Rev. Phys. 1, 112 (2019).

[23] See Supplemental Material at http://link.aps.org/supplemental/10.1103/PhysRevLett.123.216804 for details of fabrication and numerical simulations, which includes Refs. [24–26].

[24] M. Y. Sfeir, F. Wang, L. Huang, C.-C. Chuang, J. Hone, S. P. O'Brien, T. F. Heinz, and L. E. Brus, Science 306, 1540 (2004).

[25] X. M. H. Huang, R. Caldwell, L. Huang, S. C. Jun, M. Huang, M. Y. Sfeir, S. P. O'Brien, and J. Hone, Nano Lett. **5,** 1515 (2005).

[26] B.-Y. Jiang and M. M. Fogler, Phys. Rev. B **91,** 235422 (2015).

[27] J. Martin, N. Akerman, G. Ulbricht, T. Lohmann, J. H. Smet, K. von Klitzing, and A. Yacoby, Nat. Phys. **4,** 144 (2008).

[28] E. A. Laird, F. Kuemmeth, G. A. Steele, K. Grove-Rasmussen, J. Nygård, K. Flensberg, and L. P. Kouwenhoven, Rev. Mod. Phys. **87,** 703 (2015).

[29] S. Kim, I. Jo, D. C. Dillen, D. A. Ferrer, B. Fallahazad, Z. Yao, S. K. Banerjee, and E. Tutuc, Phys. Rev. Lett. **108,** 116404 (2012).

[30] K. Lee, B. Fallahazad, J. Xue, D. C. Dillen, K. Kim, T. Taniguchi, K. Watanabe, and E. Tutuc, Science **345,** 58 (2014).

[31] G. L. Yu, R. Jalil, B. Belle, A. S. Mayorov, P. Blake, F. Schedin, S. V. Morozov, L. A. Ponomarenko, F. Chiappini, S. Wiedmann, U. Zeitler, M. I. Katsnelson, A. K. Geim, K. S. Novoselov, and D. C. Elias, Proc. Natl. Acad. Sci. U.S.A. **110,** 3282 (2013).

[32] J. Tworzydło, C. W. Groth, and C. W. J. Beenakker, Phys. Rev. B **78,** 235438 (2008).

[33] A. R. Hernández and C. H. Lewenkopf, Phys. Rev. B **86,** 155439 (2012).

[34] Y. Jiang, J. Mao, D. Moldovan, M. R. Masir, G. Li, K. Watanabe, T. Taniguchi, F. M. Peeters, and E. Y. Andrei, Nat. Nanotechnol. **12,** 1045 (2017).

[35] R. R. Hartmann and M. E. Portnoi, Phys. Rev. A **89,** 012101 (2014).

[36] B.-Y. Jiang, G. X. Ni, C. Pan, Z. Fei, B. Cheng, C. N. Lau, M. Bockrath, D. N. Basov, and M. M. Fogler, Phys. Rev. Lett. **117,** 086801 (2016).

[37] S. Jung, G. M. Rutter, N. N. Klimov, D. B. Newell, I. Calizo, A. R. Hight-Walker, N. B. Zhitenev, and J. A. Stroscio, Nat. Phys. **7,** 245 (2011).

[38] J. Chae, S. Jung, A. F. Young, C. R. Dean, L. Wang, Y. Gao, K. Watanabe, T. Taniguchi, J. Hone, K. L. Shepard, P. Kim, N. B. Zhitenev, and J. A. Stroscio, Phys. Rev. Lett. **109,** 116802 (2012).

[39] S. Jung, N. Myoung, J. Park, T. Y. Jeong, H. Kim, K. Watanabe, T. Taniguchi, D. H. Ha, C. Hwang, and H. C. Park, Nano Lett. **17,** 206 (2017).

[40] D. N. Basov, M. M. Fogler, and F. J. G. d. Abajo, Science **354,** aag1992 (2016).

[41] G. X. Ni, A. S. McLeod, Z. Sun, L. Wang, L. Xiong, K. W. Post, S. S. Sunku, B.-Y. Jiang, J. Hone, C. R. Dean, M. M. Fogler, and D. N. Basov, Nature (London) **557,** 530 (2018).

[42] W. Huang, S.-J. Liang, E. Kyoseva, and L. K. Ang, Semicond. Sci. Technol. **33,** 035014 (2018).

[43] F. Khosravi, T. Van Mechelen, and Z. Jacob, Phys. Rev. B **100,** 155105 (2019).

[44] A. V. Shytov, M. I. Katsnelson, and L. S. Levitov, Phys. Rev. Lett. **99,** 246802 (2007).

[45] Y. Wang, D. Wong, A. V. Shytov, V. W. Brar, S. Choi, Q. Wu, H.-Z. Tsai, W. Regan, A. Zettl, R. K. Kawakami, S. G. Louie, L. S. Levitov, and M. F. Crommie, Science **340,** 734 (2013).

[46] J. Lu, H.-Z. Tsai, A. N. Tatan, S. Wickenburg, A. A. Omrani, D. Wong, A. Riss, E. Piatti, K. Watanabe, T. Taniguchi, A. Zettl, V. M. Pereira, and M. F. Crommie, Nat. Commun. **10,** 477 (2019).